

Hyperfine rovibrational states of H_3^+ in a weak external magnetic field

Gustavo Avila,¹ Ayaki Sunaga,¹ Stanislav Komorovsky,² and Edit Mátyus^{1,*}

¹*ELTE, Eötvös Loránd University, Institute of Chemistry,
Pázmány Péter sétány 1/A, 1117 Budapest, Hungary*

²*Institute of Inorganic Chemistry, Slovak Academy of Sciences,
Dubravska cesta 9, 84536 Bratislava, Slovakia*

(Dated: October 29, 2024)

Abstract

Rovibrational energies, wave functions, and Raman transition moments are reported for the lowest-energy states of the H_3^+ molecular ion including the magnetic couplings of the proton spins and molecular rotation in the presence of a weak external magnetic field. The rovibrational-hyperfine-Zeeman Hamiltonian matrix is constructed and diagonalized using the rovibrational eigenstates and the proton spin functions. The developed methodology can be used to compute hyperfine-Zeeman effects also for higher-energy rovibrational excitations of H_3^+ and other polyatomic molecules. These developments will guide future experiments extending quantum logic spectroscopy to polyatomic systems.

* edit.matyus@ttk.elte.hu

Recent developments in quantum technology operating on a molecular platform [1–5], have made it possible to cool and coherently manipulate single diatomic ions [1–8]. In Ref. [6], the cooling and selective quantum state preparation of the $^{40}\text{CaH}^+$ ‘spectroscopy ion’ was carried out through its entangled (quantized) translational motion within the ion trap with the $^{40}\text{Ca}^+$, ‘logic ion’. As a result, the rovibrational hyperfine-Zeeman level structure of $^{40}\text{CaH}^+$ was probed by stimulated Raman spectroscopy with unprecedented control and precision. Similar spectroscopic experiments using quantum logic [9] have already been successfully realized for $^{24}\text{MgH}^+$ [10], CaH^+ [6, 11], N_2^+ [1], and most recently, H_2^+ [8]. In principle, quantum logic spectroscopy may be extended to polyatomic systems. In this work, we develop a computational approach for modelling rovibrational-hyperfine-Zeeman effects in polyatomic systems to guide future experiments. We report the first numerical applications for the simplest polyatomic cation, H_3^+ .

The quantum mechanical motion of molecular systems has been described within the non-relativistic and Born-Openheimer (BO) approximations. These two approximations define two major fields (a) electronic structure theory, which deals with the numerical solution of the electronic Schrödinger equation; and (b) quantum nuclear motion theory, which is about the numerical solution of the rovibrational Schrödinger equation on a potential energy surface (PES). For predictions and guidance for spectroscopy, astrophysics, and potentially, quantum technology, it is useful to think about the list of rovibrational energies (wave functions) and transition moments as a ‘quantum dynamics database’ [12–16]. Then, this database, after including the necessary couplings, allows us to simulate further interactions over the relevant rovibrational subspace. The numerical solution of the (field-free) rovibrational Schrödinger equation of H_3^+ has a long history [17–21]. In this work, we go beyond the standard field-free approach by accounting for the interaction between molecular rotation, nuclear spins, and an external magnetic field, *i.e.*, we consider the nuclear spin-rotation tensor, the rotational g-tensor, the nuclear spin-spin coupling tensor, and the NMR shielding tensor in conjunction with the quantum mechanical treatment of molecular rotations and vibrations.

Regarding earlier work on hyperfine modelling, without any external magnetic field, the spin-rotation coupling was computed for rovibrational transitions of H_2D^+

and HD_2^+ [22]. The possibility of observing ortho-para transitions in the water molecule was also studied by including the spin-spin and spin-rotation coupling in the variational rovibrational computations [15, 23]. Recent work reported modelling hyperfine effects in diatomic systems of astrophysical relevance [24].

The rovibrational Schrödinger equation, $H_{\text{rv}}\psi_n = E_n\psi_n$ can be efficiently solved by replacing the laboratory-fixed (LF) Cartesian coordinates, $\mathbf{R}_i = (R_{iX}, R_{iY}, R_{iZ})$, ($i = 1, \dots, N$) of the nuclei with physically motivated internal, q_1, \dots, q_{3N-6} , orientational, $\Omega = (\alpha, \beta, \gamma)$, and overall translational coordinates corresponding to the nuclear centre of mass, $\mathbf{R}_{\text{NCM}} = \sum_{i=1}^N \frac{m_i}{m_{1\dots N}} \mathbf{R}_i$ with the m_i masses associated to the nuclei and $m_{1\dots N} = \sum_{i=1}^N m_i$. The rotational coordinates, $\Omega = (\alpha, \beta, \gamma)$, define the orientation of the the body-fixed (BF) frame through the relation [25]

$$\mathbf{R}_i = \mathbf{O}(\Omega)\mathbf{r}_i + \mathbf{R}_{\text{NCM}}, \quad i = 1, \dots, N, \quad (1)$$

where the origin of the \mathbf{r}_i body-fixed Cartesian coordinates is at the centre of mass. In what follows, capital letters $A, B = X, Y, Z$ are used for LF directions, and small letters, $a, b = x, y, z$ label BF directions. The q_1, \dots, q_{3N-6} internal coordinates are defined as scalar (and vector) products of the \mathbf{r}_i body-fixed Cartesian coordinates [26].

The rovibrational Hamiltonian is the sum of the kinetic energy operator, now written in the curvilinear Podolsky form [27], and the V potential energy depending on the internal coordinates,

$$H_{\text{rv}} = \frac{1}{2} \sum_{k=1}^{3N-3} \sum_{l=1}^{3N-3} \tilde{g}^{-1/4} \hat{p}_k G_{kl} \tilde{g}^{1/2} \hat{p}_l \tilde{g}^{-1/4} + V. \quad (2)$$

$\hat{p}_k = -i\partial/\partial q_k$ ($k = 1, \dots, 3N - 6$) is the momentum (in atomic units) conjugate to the q_k curvilinear internal coordinate, $\hat{p}_{3N-6+a} = \hat{J}_a$ ($a = 1, 2, 3$) labels the a th component of the rotational angular momentum in the body-fixed frame. $\mathbf{G} = \mathbf{g}^{-1}$ and $\tilde{g} = \det \mathbf{g}$ include the \mathbf{g} mass-weighted metric tensor corresponding to the curvilinear coordinate transformation. The Hamiltonian in Eq. (2) is understood with the simple $dV = dq_1 \dots dq_{3N-6}$ volume element for calculating integrals (the Jacobian is merged in the Hamiltonian and in the wave function). Ref. [28] reviews

further details of the formalism and the (quasi)-variational solution technique of the rovibrational Schrödinger equation as implemented in the GENIUSH program [27, 29] used in this work.

The rovibrational eigenfunctions are also eigenfunctions of the \hat{J}^2 , \hat{J}_Z rotational angular momentum operators with quantum numbers J and M , and the space inversion operator. We compute the rovibrational wave function as a linear combination of products of vibrational basis functions, $f_v(\mathbf{q})$, and the $|JKM\rangle_\Omega$ symmetric-top functions,

$$\Psi_n^{(JM)}(\Omega, \mathbf{q}) = \sum_{vK} c_{n,vK}^{(JM)} f_v(\mathbf{q}) |JKM\rangle_\Omega \quad (3)$$

with $K, M = -J, -J + 1, \dots, J - 1, J$ for all J (the Wang combinations [30] are discussed in [31]), where

$$|JKM\rangle_\Omega = \bar{D}_{MK}^{Z,J*}(\alpha, \beta, \gamma) = \sqrt{\frac{2J+1}{8\pi^2}} D_{MK}^{Z,J*}(\alpha, \beta, \gamma), \quad (4)$$

is a normalized Wigner D function (the normalization is indicated by the bar). We use the same phase conventions as Zare [25], hence the Z superscript.

The interaction of the molecular rotation and the nuclear spin magnetic moments within the system and with the external magnetic field, \mathcal{B}^{ext} , is described by the hyperfine-Zeeman Hamiltonian terms,

$$H_{\text{hf}} = - \sum_{i=1}^N \sum_{A,B=1}^3 \hat{I}_{iA} \mathcal{M}_{iA,B} \hat{J}_B + \sum_{i=1}^N \sum_{j>i}^N \sum_{A,B=1}^3 \hat{I}_{iA} (\mathcal{D}_{iA,jB} + \mathcal{R}_{iA,jB}) \hat{I}_{jB}, \quad (5)$$

$$H_Z = - \sum_{A,B=1}^3 \mu_N \hat{J}_A \mathcal{G}_{AB} \mathcal{B}_B^{\text{ext}} - \sum_{i=1}^N \sum_{A,B=1}^3 g_i \mu_N \hat{I}_{iA} (\delta_{A,B} - \sigma_{iA,B}) \mathcal{B}_B^{\text{ext}}, \quad (6)$$

which is parameterized in this work through the contributions leading order in $1/c$ [32–35]. Furthermore, in the general case, the interaction of the nuclear quadrupole moment with the electric field gradient also contributes to the hyperfine structure, but it is not relevant for the present application for H_3^+ , since the proton has a zero quadrupole moment. Furthermore, only weak external fields are considered in this

work, so higher-order magnetic effects are assumed to be negligible.

In Eqs. (5) and (6), $\mathcal{M}_{iA,B}$, $\mathcal{R}_{iA,jB}$, \mathcal{G}_{AB} , and $\sigma_{iA,B}$ are the LF elements of the nuclear spin-rotation, the indirect nuclear spin-spin coupling, the rotational g-tensor, and the magnetic shielding tensor, respectively. $\mathcal{D}_{iA,jB}$ is the direct spin-spin coupling,

$$\mathcal{D}_{iA,jB} = -\frac{g_i g_j \mu_N^2}{c^2} \left\{ \frac{1}{R_{ij}^3} \left[\frac{3R_{ij,A}R_{ij,B}}{R_{ij}^2} - \delta_{A,B} \right] + \frac{8\pi}{3} \delta(\mathbf{R}_{ij}) \right\} \quad (7)$$

with the \mathbf{R}_{ij} displacement vector of nuclei i and j in the LF frame and $R_{ij} = |\mathbf{R}_{ij}|$. The contact term proportional to $\delta(\mathbf{R}_{ij})$ is indicated but not used in the computations, since it is expected to give a negligible contribution ($< 10^{-10} \text{ cm}^{-1}$) to the hyperfine splittings. (This contact term is not directly calculable in a BO-based description, because the PES is infinite at the coalescence of two protons. For H_2^+ , $\langle \delta(\mathbf{R}_{12}) \rangle$ is available from three-body computations [36].)

The listed tensors account for couplings including the nuclear (here: proton) spin angular momenta, $\hat{\mathbf{I}}_i$, and the molecular rotational angular momentum, $\hat{\mathbf{J}}$. $\mu_N = 1/(2m_p)$ (in SI-based atomic units) is the nuclear magneton, c is the speed of light, m_p is the proton mass, and throughout this work, $g_i = g_p$ is the proton g-factor.

We aim to compute the eigenstates of the $H_{\text{rv}} + H_{\text{hf}} + H_Z$ rovibrational-hyperfine-Zeeman Hamiltonian. Since the hyperfine terms, Eq. (5), couple the rotational ($\hat{\mathbf{J}}$) and the proton spin angular momenta ($\hat{\mathbf{I}} = \hat{\mathbf{I}}_1 + \hat{\mathbf{I}}_2 + \hat{\mathbf{I}}_3$), the $\hat{\mathbf{F}}^2$ and \hat{F}_Z total angular momenta, $\hat{\mathbf{F}} = \hat{\mathbf{J}} + \hat{\mathbf{I}}$, are the conserved quantities with the quantum numbers F and M_F . If a non-zero \mathcal{B}^{ext} external magnetic field is present, which we assume to be oriented along the Z LF axis, the Zeeman terms, Eq. (6), couple different F states, only \hat{F}_Z is conserved, and M_F is the exact quantum number of the theory. We also note that for an external magnetic field, there is no space-inversion symmetry, therefore different parity states can mix.

To guide possible experimental detection of the hyperfine-Zeeman-rovibrational splittings, we compute Raman transition moments as

$$\mathcal{R} = \sum_{A,B=X,Y,Z} |\langle \Psi_f | \alpha_{AB} | \Psi_i \rangle|^2, \quad (8)$$

where α_{AB} is the (A, B) th LF component of the electric dipole polarizability operator. The hyperfine-Zeeman levels are not degenerate for the M magnetic quantum number (\hat{J}_Z), nor for the M_I spin quantum number (\hat{I}_Z). So, nuclear spin weights cannot be used, and the transition moments are explicitly computed for all pairs of the rovibrational-hyperfine-Zeeman wave functions.

First, we numerically solve the rovibrational Schrödinger equation, and then, construct the matrix representation of the rovibrational-hyperfine-Zeeman Hamiltonian. So, we need to compute the matrix elements connecting the products of the (magnetic-coupling-free) rovibrational eigenfunctions and the proton spin functions. The LF magnetic coupling matrices and the dipole polarizability matrix depend both on the orientational and the internal coordinates. To construct the matrix representation, we consider a general ‘coupling matrix’ T in the LF frame. T can be expressed with the BF-frame coupling matrix, $\mathbf{t}(\mathbf{q})$, which is computed from the molecular properties and structure, and the $\mathbf{O}(\Omega)$ orthogonal rotation matrix, which connects the LF and BF frames, Eq. (1),

$$\mathbf{T}(\Omega, \mathbf{q}) = \mathbf{O}(\Omega)\mathbf{t}(\mathbf{q})\mathbf{O}^T(\Omega) . \quad (9)$$

By exploiting this relation, we can express the orientational dependence of T using the orthonormal Wigner D -matrices, which is written for a general (non-symmetric) second-rank tensor as

$$T_{AB}(\Omega, \mathbf{q}) = \sum_{l=0}^2 \sum_{p=-l}^l \sum_{q=-l}^l \bar{D}_{pq}^{Z,l}(\Omega) \bar{T}_{lpq}^{AB}(\mathbf{q}) \quad (10)$$

for the $A, B = X, Y, Z$ LF directions. So, the angular dependence is carried by the Wigner D matrices, while $\bar{T}_{lpq}^{AB}(\mathbf{q})$ is a linear combination of the body-fixed $t_{ij}(\mathbf{q})$ ($i, j = x, y, z$) elements, which depend only on the \mathbf{q} internal coordinates. Then, we

compute the matrix elements of T with the rovibrational eigenfunctions, Eq. (3), as

$$\begin{aligned} \langle \psi_{n'}^{(J'M')} | T_{AB} | \psi_n^{(JM)} \rangle &= \sum_{K'=-J'}^{J'} \sum_{K=-J}^J \sum_{v',v} c_{n',v'K'}^{*(J'M')} c_{n,vK}^{(JM)} \\ &\sum_{l=0}^2 \sum_{p=-l}^l \sum_{q=-l}^l \langle J'K'M' | \bar{D}_{pq}^{Z,l}(\Omega) | JKM \rangle_{\Omega} \langle f_{v'}(\mathbf{q}) | \bar{T}_{lpq}^{AB}(\mathbf{q}) | f_v(\mathbf{q}) \rangle_{\mathbf{q}}. \end{aligned} \quad (11)$$

If the hyperfine-Zeeman coupling term contains an angular momentum operator factor, then, we have

$$\begin{aligned} \langle \psi_{n'}^{(J'M')} | \hat{J}_A T_{AB} | \psi_n^{(JM)} \rangle &= \sum_{K'=-J'}^{J'} \sum_{K=-J}^J c_{n',v'K'}^{*(J'M')} c_{n,vK}^{(JM)} \\ &\sum_{l=0}^2 \sum_{p=-l}^l \sum_{q=-l}^l \langle J'K'M' | \hat{J}_A \bar{D}_{pq}^{Z,l}(\Omega) | JKM \rangle_{\Omega} \langle f_{v'}(\mathbf{q}) | \bar{T}_{lpq}^{AB}(\mathbf{q}) | f_v(\mathbf{q}) \rangle_{\mathbf{q}}, \end{aligned} \quad (12)$$

where we act with \hat{J}_A on the bra and proceed with the evaluation of the sum. Alternatively, in a $T_{AB}\hat{J}_B$ -type term, we act with \hat{J}_B on the ket. Finally, we calculate the Ω integral using the known analytic integral expression of the product of three Wigner D functions (*e.g.*, Eq. 3.118 of Ref. [25]) resulting in $3j$ symbols. The integration for the internal coordinate dependence is straightforwardly computed with the quadrature used for the vibrational part of the problem. Regarding spin integration, the matrices for the spin-1/2 angular momentum components correspond to the LF frame directions and are calculated with the usual definition of the spin operators.

Regarding the computational details, the rovibrational Schrödinger equation of H_3^+ was solved using the GENIUSH program [27, 29] and the GLH3P PES [37] based on variationally optimized explicitly correlated Gaussian functions. We use the proton mass throughout this work, and we only mention that the empirical model of using different proton masses for rotation and vibration [38] had been found to provide rovibrational transition energies closer to the experimental values, which was explained by (empirically) modelling small non-adiabatic effects [39, 40], which can be derived by perturbation theory [41–44]. We use the values of the physical constants according to the CODATA 2022 recommendation [45].

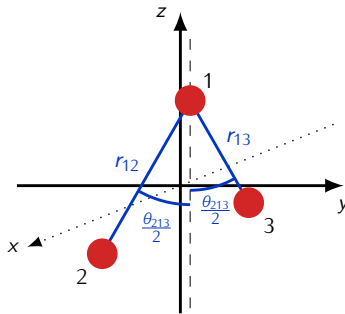


Figure 1. The internal coordinates, r_{12} , r_{13} , and θ_{213} and the x, y, z body-fixed frame axes (bisector embedding) used in the rovibrational computations of H_3^+ . The protons are fixed in the yz plane, and the origin of the frame is at the nuclear centre of mass. The body-fixed z axis is parallel with the bisector (dashed line) of the 2-1-3 proton angle.

During the rovibrational computations, we used the $(r_{12}, r_{13}, \cos \theta_{213})$ coordinates as internal coordinates and the bisector embedding as the BF frame (Fig. 1). To construct the matrix representation of the (ro)vibrational Hamiltonian, the r_{12} and r_{13} degrees of freedom were described with a potential-optimized (PO) discrete variable representation (DVR) [46, 47] based on the L_n^α associated Laguerre polynomials with $\alpha = 2$. We used Jacobi DVR, based on the $J_n^{\alpha, \beta}$ Jacobi polynomials with $\alpha = \beta = 0.05$, for the $\cos \theta_{213}$ degree of freedom. We converged all rotational energies up to $J = 3$ corresponding to the ground vibrational state to 10^{-6} cm^{-1} using the direct product grid including (61,61,91) points, which was necessary to have an unbiased assessment of all hyperfine and magnetic contributions in later steps.

For the magnetic properties [33, 48, 49], we used the CFOUR [50, 51] (and the DALTON [52, 53]) electronic structure program package(s) to compute the spin-rotation matrix [54, 55] and the rotational g matrix [56]. The nuclear magnetic shielding (NMR shielding) [57] and the indirect spin-spin coupling matrices were also determined [33, 58]. In exploratory computations, they were found to give negligibly small contributions to the rovibrational-hyperfine-Zeeman levels ($< 10^{-10} \text{ cm}^{-1}$), and hence they were neglected from the further computations. The final magnetic properties were obtained with the coupled-cluster singles and doubles (CCSD) approximation [59] and gauge-invariant atomic orbitals [33, 60]. Based on convergence tests, we used the cc-pVTZ basis set for the production runs and computed all couplings over the entire quadrature grid ($61 \times 61 \times 91 = 338\,611$ points) of the vibrational part. In this direct product grid, convergence issues were encountered

during the CCSD computation for some highly distorted geometries. In these cases, the magnetic tensors were set to zero, because the rovibrational wave functions have a very small amplitude at these extreme structures, so these points would give a negligibly small contribution to the matrix elements. For the evaluation of the rovibrational-hyperfine-Zeeman transition matrix elements, all magnetic coupling matrices computed with the electronic structure packages were rotated to the body-fixed frame (bisector embedding, Fig. 1) used in the rovibrational computations.

To construct the rovibrational-hyperfine-Zeeman Hamiltonian matrix, we used the product of the rovibrational eigenstates, including all rotational states up to $J^{\max} = 3$ corresponding to the vibrational ground state and the eight proton spin functions. This basis set included $(1 + 3 \times 3 + 5 \times 5 + 7 \times 7) \times 8 = 2\,288$ proton-spin-rovibrational functions $(K, M = -J, -J + 1, \dots, J - 1, J)$, which is also the size of the Hamiltonian matrix. To ensure strict hermiticity of the Hamiltonian matrix (the hyperfine-Zeeman terms are not in a manifestly hermitian form), the matrix representation of the spin-rotation term was computed for

$$-\sum_{i=1}^N \sum_{A,B=1}^3 \hat{I}_{iA} \mathcal{M}_{iA,B} \hat{J}_B = -\frac{1}{2} \sum_{i=1}^N \sum_{A,B=1}^3 \left[\hat{I}_{iA} \mathcal{M}_{iA,B} \hat{J}_B + \hat{J}_B \mathcal{M}_{B,iA}^T \hat{I}_{iA} \right] \quad (13)$$

similarly to Ref. [15]. All other terms were used as in Eqs. (5) and (6) and the Hamiltonian matrix fulfilled the hermiticity condition to machine precision (10^{-14}). The hyperfine-Zeeman-rotational eigenvalues and eigenvectors were computed by direct diagonalization of this matrix.

At the end of the computation, we selected the Pauli-allowed rovibrational-hyperfine-Zeeman states. Since the protons are spin-1/2 fermions, the physically relevant, rovibrational-spin wave functions transform according to the A_2 irreducible representation (irrep) of the S_3 permutation group (the subgroup of the $D_{3h}(\text{M})$ molecular symmetry group [61] excluding space inversion). So, we retained only those singly degenerate rovibrational-hyperfine-Zeeman states for which the expectation value of the ‘ P_{23} ’ permutation was -1 . For the present coordinate system (Fig. 1), $P_{23}r_{12} = r_{13}$, $P_{23}r_{13} = r_{12}$, and $P_{23}\theta_{213} = \theta_{213}$, and the transformation rules for the body-fixed frame and the symmetric-top eigenfunctions are also simple [31].

In future work, we plan to use the Pekeris coordinates [62, 63], which are linear combinations of the proton-proton distances (with independent intervals), and hence, a direct product grid using identical 1D grids is closed under all S_3 operations, so a full A_2 symmetry projector can be straightforwardly defined over the DVR grid. Alternatively, we will transform the (ro)vibrational wave function from (not PO-)DVR to the finite basis representation (FBR) and perform all necessary symmetry operations in FBR.

The dipole polarizability matrix was computed at the CCSD/aug-cc-pV5Z level of theory using the DALTON program. The matrix printed by DALTON was rotated to the bisector embedding (Fig. 1) for every nuclear geometry. The computation was repeated at every point of a direct product grid of $17 \times 17 \times 17 = 4\,913$ nuclear configurations incremented with some additional, randomly generated geometries. After discarding problematic points (close to linear configurations and large bond distances) 6 958 geometries were used to fit an analytic function, which represented the polarizability matrix with a relative error less than 0.1% [31]. This representation is expected to provide a good prediction of the hyperfine-Zeeman transitions observable with Raman spectroscopy.

The hyperfine-magnetic energies were obtained by direct diagonalization of the rovibrational-hyperfine-Zeeman Hamiltonian for a series of external magnetic field values, between 0 and 45 G (0 and 4.5 mT), and the external magnetic field was oriented along the Z LF axis. The computed hyperfine-Zeeman energies are visualized in Figures 2 and 3. The coupling between states of different rotational and total proton spin angular momentum quantum numbers, J and I , is small, so, J and I continue to be very good (approximate) quantum numbers. We observe stronger mixing for different F states at higher magnetic field strengths as shown in the lower panels of the figures, *e.g.*, for the hyperfine-Zeeman manifold of the rotational state at $\tilde{\nu} = 86.966 \text{ cm}^{-1}$.

Figure 4 presents the predicted Raman transition moments within the hyperfine-Zeeman manifolds of the $(1, 1) E'' \rightarrow (2, 1) E''$ transition at 173.240 cm^{-1} , the $(1, 0) A'_2 \rightarrow (3, 0) A'_2$ transition at 429.941 cm^{-1} , and the $(1, 1) E'' \rightarrow (3, 1) E''$ transition at 430.792 cm^{-1} . At lower fields, $|\mathcal{B}^{\text{ext}}| = 1 \text{ G}$ (0.1 mT), a simple pattern

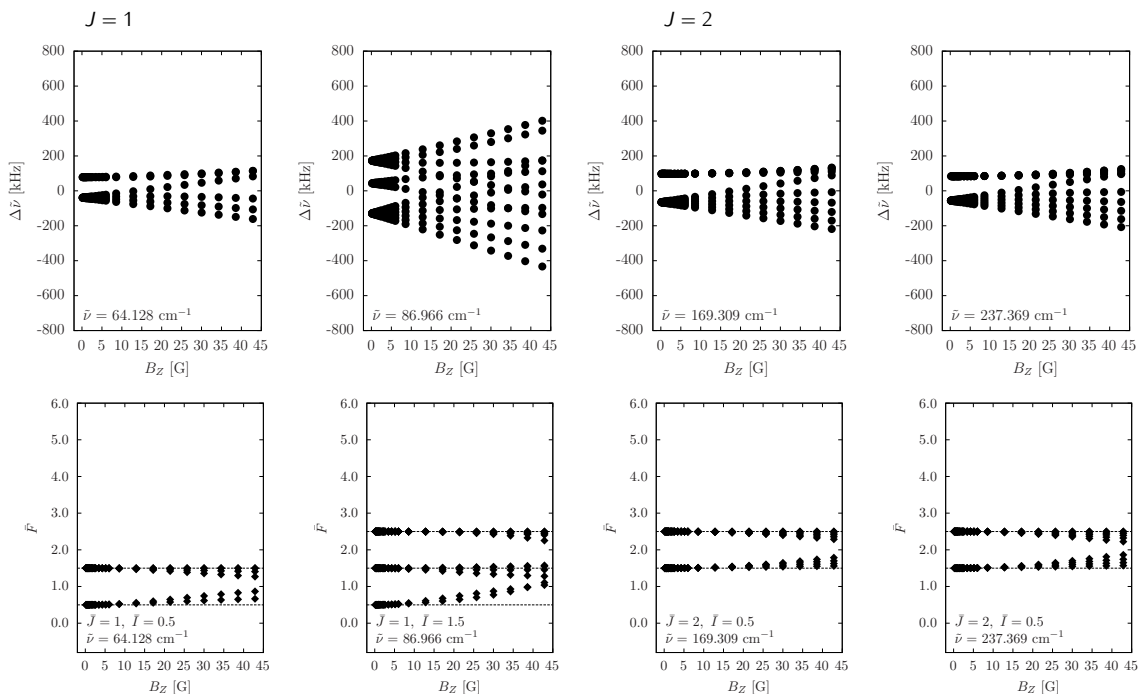


Figure 2. Hyperfine-Zeeman-rotational levels of H_3^+ corresponding to the $J = 1$ and $J = 2$ rotational states. The $\langle \hat{\mathbf{F}}^2 \rangle = \bar{F}(\bar{F} + 1)$ expectation value was computed for the actual state, and \bar{F} is plotted in the lower panels. The external magnetic field is along the Z laboratory-fixed axis, $\mathcal{B}^{\text{ext}} = (0, 0, B_Z)$.

is seen, dominated by the spin-rotation and direct spin-spin coupling. At higher fields, the transitions are split by the direct spin-magnetic and rotation-magnetic couplings. For $\mathcal{B}^{\text{ext}} = 30$ G (3 mT), we see a congested spectrum indicating multiple competing effects. The spin-rotation and rotation-magnetic couplings become more important for higher J values.

We also note that non-vanishing Raman transition moments are seen also within the hyperfine-Zeeman components within the same rotational band. As an example, Fig. 5 shows the transition moments connecting the hyperfine-Zeeman states within the $(1, 1)$ E'' (64.128 cm^{-1}) ground-state rotational manifold.

The present work reported the development of a new computational methodology to account for hyperfine-Zeeman effects in the high-resolution rovibrational spectrum of polyatomic molecules. Numerical results were presented for the simplest polyatomic system, H_3^+ , using a variational rovibrational approach and an accurate *ab initio* potential energy surface. The hyperfine-magnetic coupling matrices were

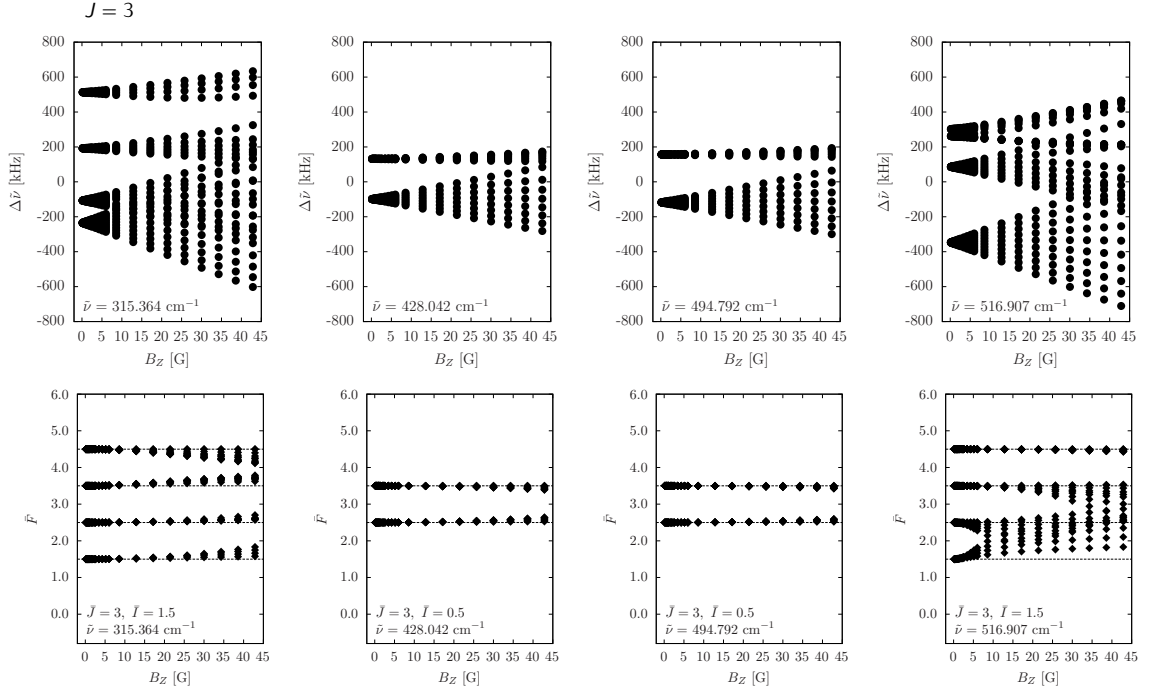


Figure 3. Hyperfine-Zeeman-rotational levels of H_3^+ corresponding to the $J = 3$ rotational states. The $\langle \hat{\mathbf{F}}^2 \rangle = \bar{F}(\bar{F} + 1)$ expectation value was computed for the actual state, and \bar{F} is plotted in the lower panels. The external magnetic field is along the Z laboratory-fixed axis, $\mathcal{B}^{\text{ext}} = (0, 0, B_Z)$.

computed by standard electronic structure theory including the leading-order contributions in $1/c$. The magnetic property computations were carried out over the vibrational grid representation to avoid fitting errors. It will be interesting to compare the computed results with future experiments. It is expected that the current results are sufficiently accurate to guide the experimental design and detection, which may be the first extension of quantum logic spectroscopy to a polyatomic system. If necessary, the present level of numerical error control and convergence of the electronic energy values underlying the potential energy surface can be further improved, and further corrections, including the leading-order regularized relativistic [64] and quantum electrodynamics corrections with precise evaluation of the Bethe logarithm [65] can be included. The precision of the current PES (based on variational explicitly correlated Gaussian computations [37]) can be further improved. Furthermore, the hyperfine-magnetic coupling matrices could also be computed using an explicitly correlated Gaussian basis representation. As to the rovibrational part, the hyperfine-Zeeman splittings can be computed for a large number of rovibrational states, since

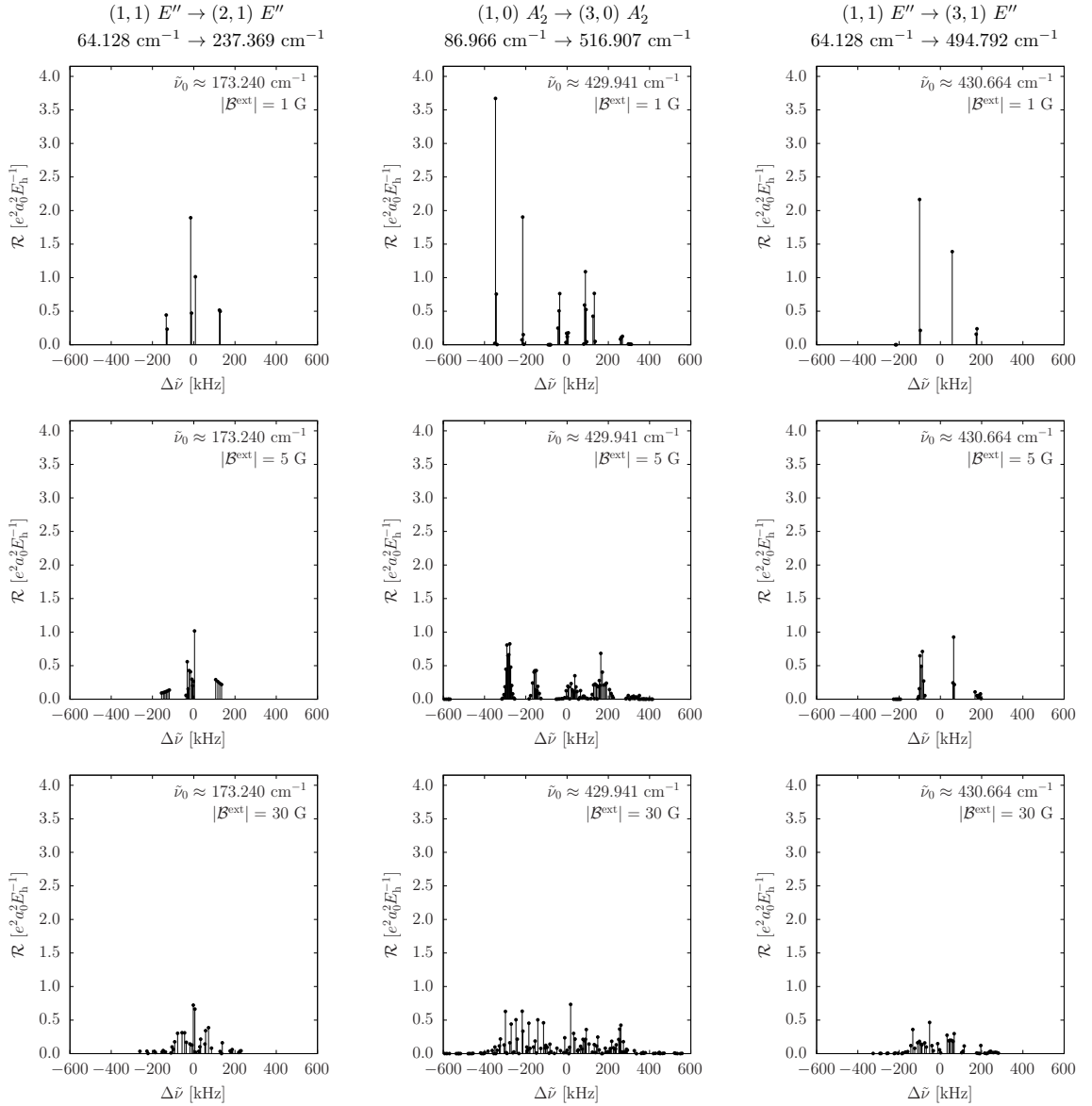


Figure 4. Raman transition moments connecting the hyperfine-Zeeman-rotational levels of H_3^+ for an external magnetic field oriented along the Z laboratory-fixed axis, $\mathcal{B}^{\text{ext}} = (0, 0, B_Z)$ with $B_Z = 1, 5$, and 30 G. The lower and upper state labels and rotational energies [31] are also shown at the top of the figure.

the integration of the property tensors with the large (gigantic) DVR grid used in this work is very accurate. Furthermore, the hyperfine-Zeeman Hamiltonian matrix, for the magnetic field values used in this work, can be efficiently diagonalized in smaller matrix blocks without losing accuracy. In this respect, it will be interesting to study the interaction of energetically close-lying (or even near degenerate) rovibrational states with different J values through the hyperfine-Zeeman couplings.

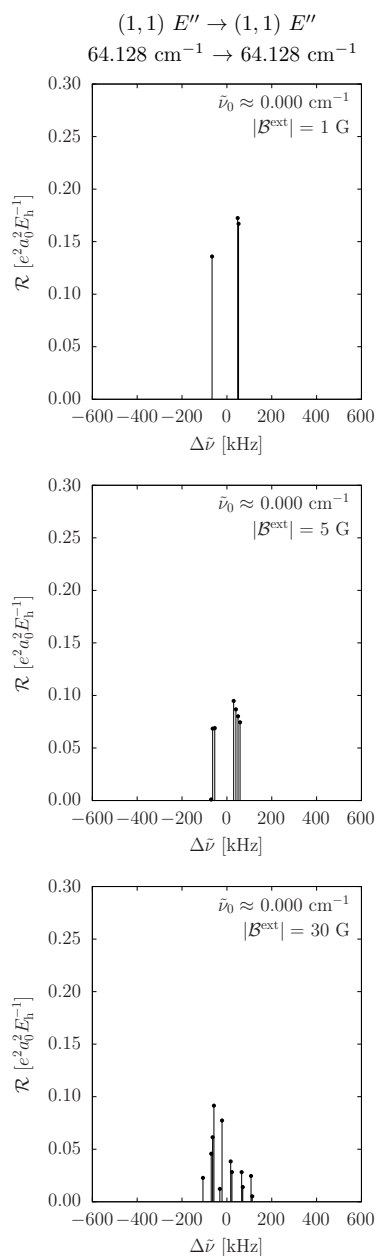


Figure 5. Raman transition moments within the hyperfine-Zeeman manifold of the rovibrational ground state, (1, 1) E'' (64.128 cm^{-1}), of H_3^+ for an external magnetic field oriented along the Z laboratory-fixed axis, $\mathcal{B}^{\text{ext}} = (0, 0, B_Z)$ with $B_Z = 1, 5$, and 30 G.

The H_3^+ molecular ion is of particular interest as the simplest polyatomic system. The computed results will be used to guide the experiments and also to test molecular quantum mechanics beyond the simplest systems, *i.e.*, H_2^+ and isotopologues [66–68]. In turn, H_3^+ , as a polyatomic species, provides orders of magnitude higher complexity due to its rich rovibrational internal structure [69], and thus, potentially high-quality data to measure and a greater variety of (rovibrational) properties to

control.

ACKNOWLEDGMENTS

Financial support of the European Research Council through a Starting Grant (No. 851421) is gratefully acknowledged. A.S. thanks the European Union’s Horizon 2022 research and innovation programme under the Marie Skłodowska-Curie Grant Agreement No. 101105452. We also thank the financial support of the Hungarian National Research, Development, and Innovation Office (FK 142869), and the Slovak Grant Agency APVV (Grant No. APVV-22-0488 to S.K.).

-
- [1] M. Sinhal, Z. Meir, K. Najafian, G. Hegi, and S. Willitsch, Quantum-nondemolition state detection and spectroscopy of single trapped molecules, [Science](#) **367**, 1213 (2020).
 - [2] K. Najafian, Z. Meir, and S. Willitsch, From megahertz to terahertz qubits encoded in molecular ions: theoretical analysis of dipole-forbidden spectroscopic transitions in N_2^+ , [Phys. Chem. Chem. Phys.](#) **22**, 23083 (2020).
 - [3] Y. Lin, D. R. Leibbrandt, D. Leibfried, and C.-W. Chou, Quantum entanglement between an atom and a molecule, [Nature](#) **581**, 273–277 (2020).
 - [4] K. Najafian, Z. Meir, M. Sinhal, and S. Willitsch, Identification of molecular quantum states using phase-sensitive forces, [Nat. Comm.](#) **11**, 4470 (2020).
 - [5] M. Sinhal and S. Willitsch, *Molecular-ion quantum technologies* (Wiley-VCH, 2023) p. 305.
 - [6] C. wen Chou, C. Kurz, D. B. Hume, P. N. Plessow, D. R. Leibbrandt, and D. Leibfried, Preparation and coherent manipulation of pure quantum states of a single molecular ion, [Nature](#) **545**, 203 (2017).
 - [7] N. Schwegler, D. Holzapfel, M. Stadler, A. Mitjans, I. Sergachev, J. P. Home, and D. Kienzler, Trapping and ground-state cooling of a single H_2^+ , [Phys. Rev. Lett.](#) **131**, 133003 (2023).

- [8] D. Holzapfel, F. Schmid, N. Schwegler, O. Stadler, M. Stadler, A. Ferck, J. P. Home, and D. Kienzler, Quantum control of a single H_2^+ molecular ion, [arXiv \(2024\)](#).
- [9] P. O. Schmidt, T. Rosenband, C. Langer, W. M. Itano, J. C. Bergquist, and D. J. Wineland, Spectroscopy using quantum logic, [Science](#) **309**, 749 (2005).
- [10] F. Wolf, Y. Wan, J. C. Heip, F. Gebert, C. Shi, and P. O. Schmidt, Non-destructive state detection for quantum logic spectroscopy of molecular ions, [Nature](#) **530**, 457 (2016).
- [11] C. W. Chou, A. L. Collopy, C. Kurz, Y. Lin, M. E. Harding, P. N. Plessow, T. Fortier, S. Diddams, D. Leibfried, and D. R. Leibbrandt, Frequency-comb spectroscopy on pure quantum states of a single molecular ion, [Science](#) **367**, 1458 (2020).
- [12] J. Tennyson, Perspective: Accurate ro-vibrational calculations on small molecules, [J. Chem. Phys.](#) **145**, 120901 (2016).
- [13] A. Owens and A. Yachmenev, RichMol: A general variational approach for rovibrational molecular dynamics in external electric fields, [J. Chem. Phys.](#) **148**, 124102 (2018).
- [14] A. G. Császár, C. Fábri, and T. Szidarovszky, Chapter 2 - Exact Numerical Methods for Stationary-State-Based Quantum Dynamics of Complex Polyatomic Molecules, in *Molecular Spectroscopy and Quantum Dynamics*, edited by R. Marquardt and M. Quack (Elsevier, 2021) pp. 43–78.
- [15] A. Yachmenev, G. Yang, E. Zak, S. Yurchenko, and J. Küpper, The nuclear-spin-forbidden rovibrational transitions of water from first principles, [J. Chem. Phys.](#) **156**, 204307 (2022).
- [16] A. Owens, E. J. Zak, K. L. Chubb, S. N. Yurchenko, J. Tennyson, and A. Yachmenev, Simulating electric field interactions with polar molecules using spectroscopic databases, [Sci. Rep.](#) **7**, 45068 (2017).
- [17] J. Tennyson and B. T. Sutcliffe, On the rovibrational levels of the H_3^+ and H_2D^+ molecules, [Mol. Phys.](#) **51**, 887 (1984).
- [18] J. Tennyson and B. T. Sutcliffe, A calculation of the rovibrational spectra of the H_3^+ , H_2D^+ and D_2H^+ molecules, [Mol. Phys.](#) **56**, 1175 (1985).
- [19] J. Tennyson and B. T. Sutcliffe, The infrared spectrum of H and its isotopomers. A challenge to theory and experiment, [J. Chem. Soc., Faraday Trans. 2](#) **82**, 1151 (1986).

- [20] M. J. Bramley and J. Carrington, Tucker, A general discrete variable method to calculate vibrational energy levels of three- and four-atom molecules, *J. Chem. Phys.* **99**, 8519 (1993).
- [21] M. J. Bramley, J. W. Tromp, J. Carrington, Tucker, and G. C. Corey, Efficient calculation of highly excited vibrational energy levels of floppy molecules: The band origins of H_3^+ up to $35\,000\text{ cm}^{-1}$, *J. Chem. Phys.* **100**, 6175 (1994).
- [22] P. Jensen, I. Paidarová, V. Špirko, and S. P. A. Sauer, Theoretical calculations of the hyperfine structure in the spectra of H_3^+ and its deuterated isotopomers, *Mol. Phys.* **91**, 319 (1997).
- [23] A. Miani and J. Tennyson, Can ortho-para transitions for water be observed?, *J. Chem. Phys.* **120**, 2732 (2004).
- [24] Q. Qu, S. N. Yurchenko, and J. Tennyson, A method for the variational calculation of hyperfine-resolved rovibronic spectra of diatomic molecules, *J. Chem. Theory Comput.* **18**, 1808 (2022).
- [25] R. N. Zare, *Angular Momentum: Understanding Spatial Aspects in Chemistry and Physics* (Wiley-Interscience, New York, 1998).
- [26] B. Sutcliffe, Coordinate Systems and Transformations, in *Handbook of Molecular Physics and Quantum Chemistry*, ed. S. Wilson. Vol. 1: *Fundamentals* (John Wiley & Sons, Ltd., 2002) Chap. 31, pp. 485–500.
- [27] E. Mátyus, G. Czakó, and A. G. Császár, Toward black-box-type full- and reduced-dimensional variational (ro)vibrational computations, *J. Chem. Phys.* **130**, 134112 (2009).
- [28] E. Mátyus, A. Martín Santa Daría, and G. Avila, Exact quantum dynamics developments for floppy molecular systems and complexes, *Chem. Commun.* **59**, 366 (2023).
- [29] C. Fábri, E. Mátyus, and A. G. Császár, Rotating full- and reduced-dimensional quantum chemical models of molecules, *J. Chem. Phys.* **134**, 074105 (2011).
- [30] S. C. Wang, On the asymmetrical top in quantum mechanics, *Phys. Rev.* **34**, 243 (1929).
- [31] See Supplemental Material for further implementation and computational details; the full list of computed hyperfine-magnetic energies, assignments and Raman transition moments are deposited in plain text files.

- [32] N. F. Ramsey, Electron coupled interactions between nuclear spins in molecules, *Phys. Rev.* **91**, 303 (1953).
- [33] T. Helgaker, M. Jaszuński, and K. Ruud, Ab initio methods for the calculation of NMR shielding and indirect spin-spin coupling constants, *Chem. Rev.* **99**, 293 (1999).
- [34] T. Helgaker, P. Jørgensen, and J. Olsen, The electronic Hamiltonian in an electromagnetic field. <https://trygvehelgaker.no/presentations/hamiltonian.pdf>.
- [35] W. H. Flygare, Magnetic interactions in molecules and an analysis of molecular electronic charge distribution from magnetic parameters, *Chem. Rev.* **74**, 653 (1974).
- [36] A. M. Frolov, Bound-state calculations of Coulomb three-body systems, *Phys. Rev. A* **59**, 4270 (1999).
- [37] M. Pavanello, L. Adamowicz, A. Alijah, N. F. Zobov, I. I. Mizus, O. L. Polyansky, J. Tennyson, T. Szidarovszky, and A. G. Császár, Calibration-quality adiabatic potential energy surfaces for H_3^+ and its isotopologues, *J. Chem. Phys.* **136**, 184303 (2012).
- [38] O. L. Polyansky and J. Tennyson, Ab initio calculation of the rotation-vibration energy levels of H_3^+ and its isotopomers to spectroscopic accuracy, *J. Chem. Phys.* **110**, 5056 (1999).
- [39] W. Kutzelnigg, Which masses are vibrating or rotating in a molecule?, *Mol. Phys.* **105**, 2627 (2007).
- [40] T. Furtenbacher, T. Szidarovszky, E. Mátyus, C. Fábri, and A. G. Császár, Analysis of the rotational-vibrational states of the molecular ion H_3^+ , *J. Chem. Theory Comput.* **9**, 5471 (2013).
- [41] E. Mátyus and S. Teufel, Effective non-adiabatic Hamiltonians for the quantum nuclear motion over coupled electronic states, *J. Chem. Phys.* **151**, 014113 (2019).
- [42] D. Ferenc and E. Mátyus, Non-adiabatic mass correction for excited states of molecular hydrogen: Improvement for the outer-well HH $^1\Sigma_g^+$ term values, *J. Chem. Phys.* **151**, 094101 (2019).
- [43] D. Ferenc, V. I. Korobov, and E. Mátyus, Nonadiabatic, relativistic, and leading-order QED corrections for rovibrational intervals of $^4\text{He}_2^+$ ($X\ ^2\Sigma_u^+$), *Phys. Rev. Lett.* **125**, 213001 (2020).
- [44] E. Mátyus and D. Ferenc, Vibronic mass computation for the EF–GK–HH $^1\Sigma_g^+$ man-

- ifold of molecular hydrogen, *Mol. Phys.* **120**, e2074905 (2022).
- [45] 2022 CODATA recommended values, fundamental constants and conversion factors, <https://physics.nist.gov/cuu/Constants/index.html> . Last accessed on 22 October 2024.
- [46] H. Wei and J. Carrington, Tucker, The discrete variable representation of a triatomic Hamiltonian in bond length–bond angle coordinates, *J. Chem. Phys.* **97**, 3029 (1992).
- [47] J. Echave and D. C. Clary, Potential optimized discrete variable representation, *Chem. Phys. Lett.* **190**, 225 (1992).
- [48] G. Cazzoli, C. Puzzarini, M. E. Harding, and J. Gauss, The hyperfine structure in the rotational spectrum of water: Lamb-dip technique and quantum-chemical calculations, *Chem. Phys. Lett.* **473**, 21 (2009).
- [49] C. Puzzarini, J. F. Stanton, and J. Gauss, Quantum-chemical calculation of spectroscopic parameters for rotational spectroscopy, *Int. Rev. Phys. Chem.* **29**, 273 (2010).
- [50] CFOUR, a molecular electronic structure program, Release v2.1 (2019), see <https://cfour.uni-mainz.de/cfour>.
- [51] D. A. Matthews, L. Cheng, M. E. Harding, F. Lipparini, S. Stopkowicz, T.-C. Jagau, P. G. Szalay, J. Gauss, and J. F. Stanton, Coupled-cluster techniques for computational chemistry: The CFOUR program package, *J. Chem. Phys.* **152**, 214108 (2020).
- [52] Dalton, a molecular electronic structure program, Release v2020.1 (2020), see <http://daltonprogram.org>.
- [53] K. Aidas, C. Angeli, K. L. Bak, V. Bakken, R. Bast, L. Boman, O. Christiansen, R. Cimiraglia, S. Coriani, P. Dahle, E. K. Dalskov, U. Ekström, T. Enevoldsen, J. J. Eriksen, P. Ettenhuber, B. Fernández, L. Ferrighi, H. Fliegl, L. Frediani, K. Hald, A. Halkier, C. Hättig, H. Heiberg, T. Helgaker, A. C. Hennum, H. Hettema, E. Hjertenæs, S. Høst, I.-M. Høyvik, M. F. Iozzi, B. Jansík, H. J. A. Jensen, D. Jonsson, P. Jørgensen, J. Kauczor, S. Kirpekar, T. Kjærgaard, W. Klopper, S. Knecht, R. Kobayashi, H. Koch, J. Kongsted, A. Krapp, K. Kristensen, A. Ligabue, O. B. Lutnæs, J. I. Melo, K. V. Mikkelsen, R. H. Myhre, C. Neiss, C. B. Nielsen, P. Norman, J. Olsen, J. M. H. Olsen, A. Osted, M. J. Packer, F. Pawłowski, T. B. Pedersen, P. F. Provasi, S. Reine, Z. Rinkevicius, T. A. Ruden, K. Ruud, V. V. Rybkin, P. Salek, C. C. M. Samson, A. S. de Merás, T. Saue, S. P. A. Sauer, B. Schimmelpfennig,

- K. Sneskov, A. H. Steindal, K. O. Sylvester-Hvid, P. R. Taylor, A. M. Teale, E. I. Tellgren, D. P. Tew, A. J. Thorvaldsen, L. Thøgersen, O. Vahtras, M. A. Watson, D. J. D. Wilson, M. Ziolkowski, and H. Ågren, The Dalton quantum chemistry program system, [WIREs Comp. Mol. Sci. 4, 269 \(2014\)](#).
- [54] J. Gauss, K. Ruud, and T. Helgaker, Perturbation-dependent atomic orbitals for the calculation of spin-rotation constants and rotational g tensors, [J. Chem. Phys. 105, 2804 \(1996\)](#).
- [55] J. Gauss and D. Sundholm, Coupled-cluster calculations of spin-rotation constants, [Mol. Phys. 91, 449 \(1997\)](#).
- [56] J. Gauss, K. Ruud, and M. Kállay, Gauge-origin independent calculation of magnetizabilities and rotational g tensors at the coupled-cluster level, [J. Chem. Phys. 127, 074101 \(2007\)](#).
- [57] J. Gauss and J. F. Stanton, Coupled-cluster calculations of nuclear magnetic resonance chemical shifts, [J. Chem. Phys. 103, 3561 \(1995\)](#).
- [58] A. A. Auer and J. Gauss, Triple excitation effects in coupled-cluster calculations of indirect spin-spin coupling constants, [J. Chem. Phys. 115, 1619 \(2001\)](#).
- [59] J. F. Stanton, J. Gauss, J. D. Watts, and R. J. Bartlett, A direct product decomposition approach for symmetry exploitation in many-body methods. I. Energy calculations, [J. Chem. Phys. 94, 4334 \(1991\)](#).
- [60] F. London, Théorie quantique des courants interatomiques dans les combinaisons aromatiques, [J. Phys. Radium 8, 397 \(1937\)](#).
- [61] P. R. Bunker and P. Jensen, *Molecular symmetry and spectroscopy, 2nd Edition* (NRC Research Press, Ottawa, 1998).
- [62] C. L. Pekeris, Ground state of two-electron atoms, [Phys. Rev. 112, 1649 \(1958\)](#).
- [63] H. Wei and J. Carrington, Tucker, Discrete variable representations of complicated kinetic energy operators, [J. Chem. Phys. 101, 1343 \(1994\)](#).
- [64] B. Rácsai, D. Ferenc, A. Margócsy, and E. Mátyus, Regularized relativistic corrections for polyelectronic and polyatomic systems with explicitly correlated Gaussians, [J. Chem. Phys. 160, 211102 \(2024\)](#).
- [65] D. Ferenc and E. Mátyus, Evaluation of the Bethe logarithm: From atom to chemical reaction, [J. Phys. Chem. A 127, 627 \(2023\)](#).

- [66] V. I. Korobov, L. Hilico, and J.-P. Karr, Hyperfine structure in the hydrogen molecular ion, *Phys. Rev. A* **74**, 040502 (2006).
- [67] J.-P. Karr, M. Haidar, L. Hilico, Z.-X. Zhong, and V. I. Korobov, Higher-order corrections to spin-spin scalar interactions in HD^+ and H_2^+ , *Phys. Rev. A* **102**, 052827 (2020).
- [68] M. Haidar, V. I. Korobov, L. Hilico, and J.-P. Karr, Higher-order corrections to spin-orbit and spin-spin tensor interactions in hydrogen molecular ions: Theory and application to H_2^+ , *Phys. Rev. A* **106**, 022816 (2022).
- [69] C. A. Bowesman, I. I. Mizus, N. F. Zobov, O. L. Polyansky, J. Sarka, B. Poirier, M. Pezzella, S. N. Yurchenko, and J. Tennyson, ExoMol line lists – L: high-resolution line lists of H_3^+ , H_2D^+ , D_2H^+ , and D_3^+ , *Mon. Not. Roy. Astron. Soc.* **519**, 6333 (2023).
- [70] Wolfram Research, Inc., Mathematica, Version 12.1, Champaign, IL, 2020.

Supplemental Material

Hyperfine rovibrational states of H_3^+ in a weak external magnetic field

Gustavo Avila,¹ Ayaki Sunaga,¹ Stanislav Komorovsky,² Edit Mátyus¹

¹ *ELTE, Eötvös Loránd University, Institute of Chemistry, Pázmány Péter sétány
1/A, 1117 Budapest, Hungary*

² *Institute of Inorganic Chemistry, Slovak Academy of Sciences, Dubravska cesta 9,
84536 Bratislava, Slovakia*

- S1. Wang functions and symmetric-top eigenfunctions
- S2. General second-rank tensors expressed with Wigner D functions
- S3. Further computational details and convergence tests
- S4. A simple analytic representation of the electric dipole polarizability matrix
- S5. Pauli-allowed states: Calculation of the effect of the P_{23} permutation operator

S1. WANG FUNCTIONS AND SYMMETRIC-TOP EIGENFUNCTIONS

In the GENIUSH program [27, 29], the rovibrational wave function is expressed as

$$\Psi_n^{(JM)}(\Omega, \mathbf{q}) = \sum_{v\tilde{K}\tau} c_{n,v\tilde{K}\tau}^{(JM)} f_v(\mathbf{q}) |J\tilde{K}\tau M\rangle_\Omega, \quad (\text{S1})$$

where $|J\tilde{K}\tau M\rangle$ labels a Wang function, which is obtained as the following linear combination of the symmetric top functions,

$$|J\tilde{K}\tau M\rangle_\Omega = \begin{cases} \frac{1}{\sqrt{2}}[|J\tilde{K}M\rangle_\Omega + |J(-\tilde{K})M\rangle_\Omega], & \text{for even } \tilde{K}, \tau = 0 \\ \frac{i}{\sqrt{2}}[|J\tilde{K}M\rangle_\Omega - |J(-\tilde{K})M\rangle_\Omega], & \text{for even } \tilde{K}, \tau = 1 \\ \frac{1}{\sqrt{2}}[|J\tilde{K}M\rangle_\Omega - |J(-\tilde{K})M\rangle_\Omega], & \text{for odd } \tilde{K}, \tau = 0 \\ \frac{i}{\sqrt{2}}[|J\tilde{K}M\rangle_\Omega + |J(-\tilde{K})M\rangle_\Omega], & \text{for odd } \tilde{K}, \tau = 1 \end{cases} \quad (\text{S2})$$

with $M = -J, -J + 1, \dots, J - 1, J$, $\tilde{K} = 0, 1, \dots, J$, $\tau = 0, 1$. For $\tilde{K} = 0$ there is only $\tau = 0$ with $|J, \tilde{K} = 0, \tau = 0, M\rangle_\Omega = |J00\rangle_\Omega$.

This linear combination of the symmetric top functions ensures that all rovibrational Hamiltonian matrix elements are real. The symmetric top eigenfunctions are, $K, M = -J, -J + 1, \dots, J - 1, J$,

$$|JKM\rangle_\Omega = \bar{D}_{MK}^{Z,J*}(\alpha, \beta, \gamma) = \sqrt{\frac{2J+1}{8\pi^2}} D_{MK}^{Z,J*}(\alpha, \beta, \gamma), \quad (\text{S3})$$

and we also note that

$$\bar{D}_{M,K}^{Z,J}(\Omega) = (-1)^{M-K} \bar{D}_{-M,-K}^{Z,J*}(\Omega). \quad (\text{S4})$$

S2. GENERAL SECOND-RANK TENSORS EXPRESSED WITH WIGNER D FUNCTIONS

The laboratory-frame property tensors are connected to their body-fixed frame versions through transformation with the rotation matrix defined as [25]

$$\mathbf{O}(\alpha, \beta, \gamma) = \mathbf{O}_1(\alpha) \mathbf{O}_2(\beta) \mathbf{O}_3(\gamma) \quad (\text{S5})$$

with

$$\mathbf{O}_1(\alpha) = \begin{pmatrix} \cos \alpha & -\sin \alpha & 0 \\ \sin \alpha & \cos \alpha & 0 \\ 0 & 0 & 1 \end{pmatrix}, \quad \mathbf{O}_2(\beta) = \begin{pmatrix} \cos \beta & 0 & \sin \beta \\ 0 & 1 & 0 \\ -\sin \beta & 0 & \cos \beta \end{pmatrix}, \quad \mathbf{O}_3(\gamma) = \begin{pmatrix} \cos \gamma & -\sin \gamma & 0 \\ \sin \gamma & \cos \gamma & 0 \\ 0 & 0 & 1 \end{pmatrix}. \quad (\text{S6})$$

Then,

$$\mathbf{T}(\Omega, \mathbf{q}) = \mathbf{O}(\Omega) \mathbf{t}(\mathbf{q}) \mathbf{O}^T(\Omega). \quad (\text{S7})$$

This orientational dependence of a second-rank tensor is conveniently expressed using the Wigner D functions as

$$T_{AB}(\Omega, \mathbf{q}) = \sum_{l=0}^2 \sum_{p=-l}^l \sum_{q=-l}^l \bar{D}_{pq}^{Z,l}(\Omega) \bar{T}_{lpq}^{AB}(\mathbf{q}), \quad (\text{S8})$$

where $A, B = X, Y, Z$ label laboratory-frame coordinates and we use the normalized Wigner D functions, $\bar{D}_{M,K}^{Z,J}(\Omega)$. In Eq. (S8), $\bar{T}_{lpq}^{AB}(\mathbf{q})$ can be expressed as a linear combination of the body-fixed $t_{ij}(\mathbf{q})$ values. These expressions are known in the literature, but different phase conventions exist, so for full consistency within our work, we calculated the decomposition terms with Wolfram Mathematica [70] by exploiting the orthonormality of the $\bar{D}_{M,K}^{Z,J}$ functions,

$$\begin{aligned} \bar{T}_{lpq}^{AB}(\mathbf{q}) &= \int_0^{2\pi} d\alpha \int_0^\pi \sin \beta \, d\beta \int_0^{2\pi} d\gamma \, \bar{D}_{pq}^{Z,l*}(\alpha, \beta, \gamma) T_{AB}(\alpha, \beta, \gamma, \mathbf{q}) \\ &= \int_0^{2\pi} d\alpha \int_0^\pi \sin \beta \, d\beta \int_0^{2\pi} d\gamma \, \bar{D}_{pq}^{Z,l*}(\alpha, \beta, \gamma) [\mathbf{O}(\alpha, \beta, \gamma) \mathbf{t}(\mathbf{q}) \mathbf{O}^T(\alpha, \beta, \gamma)]_{AB} \\ &= \int_0^{2\pi} d\alpha \int_0^\pi \sin \beta \, d\beta \int_0^{2\pi} d\gamma \, \bar{D}_{pq}^{Z,l*}(\alpha, \beta, \gamma) \sum_{a,b} O_{Aa}(\alpha, \beta, \gamma) t_{ab}(\mathbf{q}) O_{Bb}(\alpha, \beta, \gamma). \end{aligned} \quad (\text{S9})$$

We also note that the phase convention in Zare's book (indicated with the 'Z' superscript) [25] is related to the Wigner D function implementation in Wolfram Mathe-

matica (indicated with the ‘M’ superscript) as

$$D_{M,K}^{Z,J}(\alpha, \beta, \gamma) = (-1)^{M-K} D_{K,M}^{M,J}(-\alpha, \beta, -\gamma). \quad (\text{S10})$$

For the sake of completeness, the result of this calculation for a general (non-symmetric) T tensor is listed as follows. We used these expressions in our Fortran implementation. The expressions can be simplified for a symmetric tensor (*e.g.*, the polarizability tensor).

$$\begin{aligned}
\bar{T}_{0,0,0}^{X,X} &= (2\sqrt{2}(t_{x,x} + t_{y,y} + t_{z,z})\pi)/3 \\
\bar{T}_{2,-2,-2}^{X,X} &= ((t_{x,x} + i(t_{x,y} + t_{y,x} + t_{x,x} + it_{y,y}))\pi)/\sqrt{10} \\
\bar{T}_{2,-2,-1}^{X,X} &= ((t_{x,z} + it_{y,z} + t_{z,x} + it_{z,y})\pi)/\sqrt{10} \\
\bar{T}_{2,-2,0}^{X,X} &= -(((t_{x,x} + t_{y,y} - 2t_{z,z})\pi)/\sqrt{15}) \\
\bar{T}_{2,-2,1}^{X,X} &= -(((t_{x,z} - i(t_{y,z} + it_{z,x} + t_{z,y}))\pi)/\sqrt{10}) \\
\bar{T}_{2,-2,2}^{X,X} &= ((t_{x,x} - i(t_{x,y} + t_{y,x} - it_{y,y}))\pi)/\sqrt{10} \\
\bar{T}_{2,0,-2}^{X,X} &= -(((t_{x,x} + i(t_{x,y} + t_{y,x} + it_{y,y}))\pi)/\sqrt{15}) \\
\bar{T}_{2,0,-1}^{X,X} &= -(((t_{x,z} + it_{y,z} + t_{z,x} + it_{z,y})\pi)/\sqrt{15}) \\
\bar{T}_{2,0,0}^{X,X} &= (\sqrt{2/5}(t_{x,x} + t_{y,y} - 2t_{z,z})\pi)/3 \\
\bar{T}_{2,0,1}^{X,X} &= ((t_{x,z} - i(t_{y,z} + it_{z,x} + t_{z,y}))/\sqrt{15}) \\
\bar{T}_{2,0,2}^{X,X} &= ((-t_{x,x} + i(t_{x,y} + t_{y,x}) + t_{y,y})\pi)/\sqrt{15} \\
\bar{T}_{2,2,-2}^{X,X} &= ((t_{x,x} + i(t_{x,y} + t_{y,x} + it_{y,y}))\pi)/\sqrt{10} \\
\bar{T}_{2,2,-1}^{X,X} &= ((t_{x,z} + it_{y,z} + t_{z,x} + it_{z,y})\pi)/\sqrt{10} \\
\bar{T}_{2,2,0}^{X,X} &= -(((t_{x,x} + t_{y,y} - 2t_{z,z})\pi)/\sqrt{15}) \\
\bar{T}_{2,2,1}^{X,X} &= -(((t_{x,z} - i(t_{y,z} + it_{z,x} + t_{z,y}))\pi)/\sqrt{10}) \\
\bar{T}_{2,-2,2}^{X,X} &= ((t_{x,x} - i(t_{x,y} + t_{y,x}) - t_{y,y})\pi)/\sqrt{10}
\end{aligned} \quad (\text{S11})$$

$$\begin{aligned}
\bar{T}_{1,0,-1}^{X,Y} &= ((-it_{x,z} + t_{y,z} + it_{z,x} - t_{z,y})\pi)/\sqrt{3} \\
\bar{T}_{1,0,0}^{X,Y} &= \sqrt{2/3}(t_{x,y} - t_{y,x})\pi \\
\bar{T}_{1,0,1}^{X,Y} &= ((-it_{x,z} - t_{y,z} + it_{z,x} + t_{z,y})\pi)/\sqrt{3} \\
\bar{T}_{2,-2,-2}^{X,Y} &= ((-it_{x,x} + t_{x,y} + t_{y,x} + it_{y,y})\pi)/\sqrt{10} \\
\bar{T}_{2,-2,-1}^{X,Y} &= ((-it_{x,z} + t_{y,z} - it_{z,x} + t_{z,y})\pi)/\sqrt{10} \\
\bar{T}_{2,-2,0}^{X,Y} &= (i(t_{x,x} + t_{y,y} - 2t_{z,z})\pi)/\sqrt{15} \\
\bar{T}_{2,-2,1}^{X,Y} &= ((it_{x,z} + t_{y,z} + it_{z,x} + t_{z,y})\pi)/\sqrt{10} \\
\bar{T}_{2,-2,2}^{X,Y} &= (-i(t_{x,x} - i(t_{x,y} + t_{y,x}) - t_{y,y})\pi)/\sqrt{10} \\
\bar{T}_{2,2,-2}^{X,Y} &= -(((-it_{x,x} + t_{x,y} + t_{y,x} + it_{y,y})\pi)/\sqrt{10}) \\
\bar{T}_{2,2,-1}^{X,Y} &= (i(t_{x,z} + it_{y,z} + t_{z,x} + it_{z,y})\pi)/\sqrt{10} \\
\bar{T}_{2,2,0}^{X,Y} &= (-i(t_{x,x} + t_{y,y} - 2t_{z,z})\pi)/\sqrt{15} \\
\bar{T}_{2,2,1}^{X,Y} &= (-it_{x,z}\pi - (t_{y,z} + it_{z,x} + t_{z,y})\pi)/\sqrt{10} \\
\bar{T}_{2,2,2}^{X,Y} &= ((it_{x,x} + t_{x,y} + t_{y,x} - it_{y,y})\pi)/\sqrt{10}
\end{aligned} \tag{S12}$$

$$\begin{aligned}
\bar{T}_{1,-1,-1}^{X,Z} &= ((t_{x,z} + i(t_{y,x} + it_{z,x} - t_{z,y}))\pi)/\sqrt{6} \\
\bar{T}_{1,-1,0}^{X,Z} &= (i(t_{x,y} - t_{y,x})\pi)/\sqrt{3} \\
\bar{T}_{1,-1,1}^{X,Z} &= ((t_{x,z} - it_{y,x} - t_{z,x} + it_{z,y})\pi)/\sqrt{6} \\
\bar{T}_{1,1,-1}^{X,Z} &= ((t_{x,z} + i(t_{y,z} + it_{z,x} - t_{z,y}))\pi)/\sqrt{6} \\
\bar{T}_{1,1,0}^{X,Z} &= (i(t_{x,y} - t_{y,x})\pi)/\sqrt{3} \\
\bar{T}_{1,1,1}^{X,Z} &= ((t_{x,z} - it_{y,z} - t_{z,x} + it_{z,y})\pi)/\sqrt{6} \\
\bar{T}_{2,-1,-2}^{X,Z} &= ((t_{x,x} + i(t_{x,y} + t_{y,x} + it_{y,y}))\pi)/\sqrt{10} \\
\bar{T}_{2,-1,-1}^{X,Z} &= ((t_{x,z} + it_{y,z} + t_{z,x} + it_{z,y})\pi)/\sqrt{10} \\
\bar{T}_{2,-1,0}^{X,Z} &= -(((t_{x,x} + t_{y,y} - 2t_{z,z})\pi)/\sqrt{15}) \\
\bar{T}_{2,-1,1}^{X,Z} &= -(((t_{x,z} - i(t_{y,z} + it_{z,x} + t_{z,y}))\pi)/\sqrt{10}) \\
\bar{T}_{2,-1,2}^{X,Z} &= ((t_{x,x} - i(t_{x,y} + t_{y,x} - it_{y,y}))\pi)/\sqrt{10} \\
\bar{T}_{1,1,-2}^{X,Z} &= -(((t_{x,x} + i(t_{x,y} + t_{y,x} + it_{y,y}))\pi)/\sqrt{10}) \\
\bar{T}_{1,1,-1}^{X,Z} &= -(((t_{x,z} + it_{y,z} + t_{z,x} + it_{z,y})\pi)/\sqrt{10}) \\
\bar{T}_{1,1,0}^{X,Z} &= ((t_{x,x} + t_{y,y} - 2t_{z,z})\pi)/\sqrt{15} \\
\bar{T}_{1,1,1}^{X,Z} &= ((t_{x,z} - i(t_{y,z} + it_{z,x} + t_{z,y}))\pi)/\sqrt{10} \\
\bar{T}_{1,1,2}^{X,Z} &= ((-t_{x,x} + i(t_{x,y} + t_{y,x}) + t_{y,y})\pi)/\sqrt{10}
\end{aligned} \tag{S13}$$

$$\begin{aligned}
\bar{T}_{1,0,-1}^{Y,X} &= ((it_{x,z} - t_{y,z} - it_{z,x} + t_{z,y})\pi)/\sqrt{3} \\
\bar{T}_{1,0,0}^{Y,X} &= \sqrt{2/3}(-t_{x,y} + t_{y,x})\pi \\
\bar{T}_{1,0,1}^{Y,X} &= ((it_{x,z} + t_{y,z} - it_{z,x} - t_{z,y})\pi)/\sqrt{3} \\
\bar{T}_{2,-2,-2}^{Y,X} &= ((-it_{x,x} + t_{x,y} + t_{y,x} + it_{y,y})\pi)/\sqrt{10} \\
\bar{T}_{2,-2,-1}^{Y,X} &= ((-it_{x,z} + t_{y,z} - it_{z,x} + t_{z,y})\pi)/\sqrt{10} \\
\bar{T}_{2,-2,0}^{Y,X} &= (i(t_{x,x} + t_{y,y} - 2t_{z,z})\pi)/\sqrt{15} \\
\bar{T}_{2,-2,1}^{Y,X} &= ((it_{x,z} + t_{y,z} + it_{z,x} + t_{z,y})\pi)/\sqrt{10} \\
\bar{T}_{2,-2,2}^{Y,X} &= (-i(t_{x,x} - i(t_{x,y} + t_{y,x}) - t_{y,y})\pi)/\sqrt{10} \\
\bar{T}_{2,2,-1}^{Y,X} &= -(((-it_{x,x} + t_{x,y} + t_{y,x} + it_{y,y})\pi)/\sqrt{10}) \\
\bar{T}_{2,2,-1}^{Y,X} &= (i(t_{x,z} + it_{y,z} + t_{z,x} + it_{z,y})\pi)/\sqrt{10} \\
\bar{T}_{2,2,-1}^{Y,X} &= (-i(t_{x,x} + t_{y,y} - 2t_{z,z})\pi)/\sqrt{15} \\
\bar{T}_{2,2,-1}^{Y,X} &= (-it_{x,z}\pi - (t_{y,z} + it_{z,x} + t_{z,y})\pi)/\sqrt{10} \\
\bar{T}_{2,2,-1}^{Y,X} &= ((it_{x,x} + t_{x,y} + t_{y,x} - it_{y,y})\pi)/\sqrt{10}
\end{aligned} \tag{S14}$$

$$\begin{aligned}
\bar{T}_{0,0,0}^{Y,Y} &= (2\sqrt{2}(t_{x,x} + t_{y,y} + t_{z,z})\pi)/3 \\
\bar{T}_{2,-2,-2}^{Y,Y} &= -(((t_{x,x} + i(t_{x,y} + t_{y,x} + it_{y,y})))\pi)/\sqrt{10} \\
\bar{T}_{2,-2,-1}^{Y,Y} &= -(((t_{x,z} + it_{y,z} + t_{z,x} + it_{z,y}))\pi)/\sqrt{10} \\
\bar{T}_{2,-2,0}^{Y,Y} &= ((t_{x,x} + t_{y,y} - 2t_{z,z})\pi)/\sqrt{15} \\
\bar{T}_{2,-2,1}^{Y,Y} &= ((t_{x,z} - i(t_{y,z} + it_{z,x} + t_{z,y}))\pi)/\sqrt{10} \\
\bar{T}_{2,-2,2}^{Y,Y} &= -(((t_{x,x} - i(t_{x,y} + t_{y,x}) - t_{y,y})\pi)/\sqrt{10} \\
\bar{T}_{2,0,-2}^{Y,Y} &= -(((t_{x,x} + i(t_{x,y} + t_{y,x} + it_{y,y})))\pi)/\sqrt{15} \\
\bar{T}_{2,0,-1}^{Y,Y} &= -(((t_{x,z} + it_{y,z} + t_{z,x} + it_{z,y}))\pi)/\sqrt{15} \\
\bar{T}_{2,0,0}^{Y,Y} &= (\sqrt{2/5}(t_{x,x} + t_{y,y} - 2t_{z,z})\pi)/3 \\
\bar{T}_{2,0,1}^{Y,Y} &= ((t_{x,z} - i(t_{y,z} + it_{z,x} + t_{z,y}))\pi)/\sqrt{15} \\
\bar{T}_{2,0,2}^{Y,Y} &= -(((t_{x,x} - i(t_{x,y} + t_{y,x}) - t_{y,y})\pi)/\sqrt{15} \\
\bar{T}_{2,2,-1}^{Y,Y} &= -(((t_{x,x} + i(t_{x,y} + t_{y,x} + it_{y,y})))\pi)/\sqrt{10} \\
\bar{T}_{2,2,-2}^{Y,Y} &= -(((t_{x,z} + it_{y,z} + t_{z,x} + it_{z,y}))\pi)/\sqrt{10} \\
\bar{T}_{2,2,0}^{Y,Y} &= ((t_{x,x} + t_{y,y} - 2t_{z,z})\pi)/\sqrt{15} \\
\bar{T}_{2,2,1}^{Y,Y} &= ((t_{x,z} - i(t_{y,z} + it_{z,x} + t_{z,y}))\pi)/\sqrt{10} \\
\bar{T}_{2,2,2}^{Y,Y} &= ((-t_{x,x} + i(t_{x,y} + t_{y,x}) + t_{y,y})\pi)/\sqrt{10}
\end{aligned} \tag{S15}$$

$$\begin{aligned}
\bar{T}_{2,-1,-1}^{Y,Z} &= ((-it_{x,z} + t_{y,z} + it_{z,x} - t_{z,y})\pi)/\sqrt{6} \\
\bar{T}_{2,-1,0}^{Y,Z} &= ((t_{x,y} - t_{y,x})\pi)/\sqrt{3} \\
\bar{T}_{2,-1,1}^{Y,Z} &= ((-it_{x,z} - t_{y,z} + it_{z,x} + t_{z,y})\pi)/\sqrt{6} \\
\bar{T}_{1,1,-1}^{Y,Z} &= ((it_{x,z} - t_{y,z} - it_{z,x} + t_{z,y})\pi)/\sqrt{6} \\
\bar{T}_{1,1,0}^{Y,Z} &= ((-t_{x,y} + t_{y,x})\pi)/\sqrt{3} \\
\bar{T}_{1,1,1}^{Y,Z} &= ((it_{x,z} + t_{y,z} - it_{z,x} - t_{z,y})\pi)/\sqrt{6} \\
\bar{T}_{2,-1,-2}^{Y,Z} &= ((-it_{x,x} + t_{x,y} + t_{y,x} + it_{y,y})\pi)/\sqrt{10} \\
\bar{T}_{2,-1,-1}^{Y,Z} &= ((-it_{x,z} + t_{y,z} - it_{z,x} + t_{z,y})\pi)/\sqrt{10} \\
\bar{T}_{2,-1,0}^{Y,Z} &= (i(t_{x,x} + t_{y,y} - 2t_{z,z})\pi)/\sqrt{15} \\
\bar{T}_{2,-1,1}^{Y,Z} &= ((it_{x,z} + t_{y,z} + it_{z,x} + t_{z,y})\pi)/\sqrt{10} \\
\bar{T}_{2,-1,2}^{Y,Z} &= (-i(t_{x,x} - i(t_{x,y} + t_{y,x} - it_{y,y}))\pi)/\sqrt{10} \\
\bar{T}_{2,1,-2}^{Y,Z} &= ((-it_{x,x} + t_{x,y} + t_{y,x} + it_{y,y})\pi)/\sqrt{10} \\
\bar{T}_{2,1,-1}^{Y,Z} &= ((-it_{x,z} + t_{y,z} - it_{z,x} + t_{z,y})\pi)/\sqrt{10} \\
\bar{T}_{2,1,0}^{Y,Z} &= (i(t_{x,x} + t_{y,y} - 2t_{z,z})\pi)/\sqrt{15} \\
\bar{T}_{2,1,1}^{Y,Z} &= ((it_{x,z} + t_{y,z} + it_{z,x} + t_{z,y})\pi)/\sqrt{10} \\
\bar{T}_{2,1,2}^{Y,Z} &= (-i(t_{x,x} - i(t_{x,y} + t_{y,x}) - t_{y,y})\pi)/\sqrt{10}
\end{aligned} \tag{S16}$$

$$\begin{aligned}
\bar{T}_{1,-1,-1}^{Z,X} &= ((-t_{x,z} - it_{y,z} + t_{z,x} + it_{z,y})\pi)/\sqrt{6} \\
\bar{T}_{1,-1,0}^{Z,X} &= (-i(t_{x,y} - t_{y,x})\pi)/\sqrt{3} \\
\bar{T}_{1,-1,1}^{Z,X} &= ((-t_{x,z} + it_{y,z} + t_{z,x} - it_{z,y})\pi)/\sqrt{6} \\
\bar{T}_{1,1,-1}^{Z,X} &= ((-t_{x,z} - it_{y,z} + t_{z,x} + it_{z,y})\pi)/\sqrt{6} \\
\bar{T}_{1,1,0}^{Z,X} &= (-i(t_{x,y} - t_{y,x})\pi)/\sqrt{3} \\
\bar{T}_{1,1,1}^{Z,X} &= ((-t_{x,z} + it_{y,z} + t_{z,x} - it_{z,y})\pi)/\sqrt{6} \\
\bar{T}_{2,-1,-2}^{Z,X} &= ((t_{x,x} + i(t_{x,y} + t_{y,x} + it_{y,y}))\pi)/\sqrt{10} \\
\bar{T}_{2,-1,-1}^{Z,X} &= ((t_{x,z} + it_{y,z} + t_{z,x} + it_{z,y})\pi)/\sqrt{10} \\
\bar{T}_{2,-1,0}^{Z,X} &= -(((t_{x,x} + t_{y,y} - 2t_{z,z})\pi)/\sqrt{15}) \\
\bar{T}_{2,-1,1}^{Z,X} &= -(((t_{x,z} - i(t_{y,z} + it_{z,x} + t_{z,y}))\pi)/\sqrt{10}) \\
\bar{T}_{2,-1,2}^{Z,X} &= ((t_{x,x} - i(t_{x,y} + t_{y,x} - it_{y,y}))\pi)/\sqrt{10} \\
\bar{T}_{2,1,-2}^{Z,X} &= -(((t_{x,x} + i(t_{x,y} + t_{y,x} + it_{y,y}))\pi)/\sqrt{10}) \\
\bar{T}_{2,1,-1}^{Z,X} &= -(((t_{x,z} + it_{y,z} + t_{z,x} + it_{z,y})\pi)/\sqrt{10}) \\
\bar{T}_{2,1,0}^{Z,X} &= ((t_{x,x} + t_{y,y} - 2t_{z,z})\pi)/\sqrt{15} \\
\bar{T}_{2,1,1}^{Z,X} &= ((t_{x,z} - i(t_{y,z} + it_{z,x} + t_{z,y}))\pi)/\sqrt{10} \\
\bar{T}_{2,1,2}^{Z,X} &= ((-t_{x,x} + i(t_{x,y} + t_{y,x}) + t_{y,y})\pi)/\sqrt{10}
\end{aligned} \tag{S17}$$

$$\begin{aligned}
\bar{T}_{1,-1,-1}^{Z,Y} &= ((it_{x,z} - t_{y,z} - it_{z,x} + t_{z,y})\pi)/\sqrt{6} \\
\bar{T}_{1,-1,0}^{Z,Y} &= ((-t_{x,y} + t_{y,x})\pi)/\sqrt{3} \\
\bar{T}_{1,-1,1}^{Z,Y} &= ((it_{x,z} + t_{y,z} - it_{z,x} - t_{z,y})\pi)/\sqrt{6} \\
\bar{T}_{1,1,-1}^{Z,Y} &= ((-it_{x,z} + t_{y,z} + it_{z,x} - t_{z,y})\pi)/\sqrt{6} \\
\bar{T}_{1,1,0}^{Z,Y} &= ((t_{x,y} - t_{y,x})\pi)/\sqrt{3} \\
\bar{T}_{1,1,1}^{Z,Y} &= ((-it_{x,z} - t_{y,z} + it_{z,x} + t_{z,y})\pi)/\sqrt{6} \\
\bar{T}_{2,-1,-2}^{Z,Y} &= ((-it_{x,x} + t_{x,y} + t_{y,x} + it_{y,y})\pi)/\sqrt{10} \\
\bar{T}_{2,-1,-1}^{Z,Y} &= ((-it_{x,z} + t_{y,z} - it_{z,x} + t_{z,y})\pi)/\sqrt{10} \\
\bar{T}_{2,-1,0}^{Z,Y} &= (i(t_{x,x} + t_{y,y} - 2t_{z,z})\pi)/\sqrt{15} \\
\bar{T}_{2,-1,1}^{Z,Y} &= ((it_{x,z} + t_{y,z} + it_{z,x} + t_{z,y})\pi)/\sqrt{10} \\
\bar{T}_{2,-1,2}^{Z,Y} &= (-i(t_{x,x} - i(t_{x,y} + t_{y,x} - it_{y,y}))\pi)/\sqrt{10} \\
\bar{T}_{2,1,-2}^{Z,Y} &= ((-it_{x,x} + t_{x,y} + t_{y,x} + it_{y,y})\pi)/\sqrt{10} \\
\bar{T}_{2,1,-1}^{Z,Y} &= ((-it_{x,z} + t_{y,z} - it_{z,x} + t_{z,y})\pi)/\sqrt{10} \\
\bar{T}_{2,1,0}^{Z,Y} &= (i(t_{x,x} + t_{y,y} - 2t_{z,z})\pi)/\sqrt{15} \\
\bar{T}_{2,1,1}^{Z,Y} &= ((it_{x,z} + t_{y,z} + it_{z,x} + t_{z,y})\pi)/\sqrt{10} \\
\bar{T}_{2,1,2}^{Z,Y} &= (-i(t_{x,x} - i(t_{x,y} + t_{y,x}) - t_{y,y})\pi)/\sqrt{10} \tag{S18}
\end{aligned}$$

$$\begin{aligned}
\bar{T}_{0,0,0}^{Z,Z} &= (2\sqrt{2}(t_{x,x} + t_{y,y} + t_{z,z})\pi)/3 \\
\bar{T}_{2,0,-2}^{Z,Z} &= (2(t_{x,x} + i(t_{x,y} + t_{y,x} + it_{y,y}))\pi)/\sqrt{15} \\
\bar{T}_{2,0,-1}^{Z,Z} &= (2(t_{x,z} + it_{y,z} + t_{z,x} + it_{z,y})\pi)/\sqrt{15} \\
\bar{T}_{2,0,0}^{Z,Z} &= (-2\sqrt{2/5}(t_{x,x} + t_{y,y} - 2t_{z,z})\pi)/3 \\
\bar{T}_{2,0,1}^{Z,Z} &= (-2(t_{x,z} - i(t_{y,z} + it_{z,x} + t_{z,y}))\pi)/\sqrt{15} \\
\bar{T}_{2,0,2}^{Z,Z} &= (2(t_{x,x} - i(t_{x,y} + t_{y,x} - it_{y,y}))\pi)/\sqrt{15} \tag{S19}
\end{aligned}$$

During the calculations, the product of three Wigner D functions are integrated

according to the known relation, Eq. 3.118 of Ref. [25],

$$\begin{aligned} & \int_0^{2\pi} d\alpha \int_0^\pi \sin \beta \, d\beta \int_0^{2\pi} d\gamma \, D_{M_3, K_3}^{Z, J_3}(\alpha, \beta, \gamma) D_{M_2, K_2}^{Z, J_2}(\alpha, \beta, \gamma) D_{M_1, K_1}^{Z, J_1}(\alpha, \beta, \gamma) \\ &= 8\pi^2 \begin{pmatrix} J_1 & J_2 & J_3 \\ M_1 & M_2 & M_3 \end{pmatrix} \begin{pmatrix} J_1 & J_2 & J_3 \\ K_1 & K_2 & K_3 \end{pmatrix} \end{aligned} \quad (\text{S20})$$

expressed with 3j symbols.

Furthermore, the action of the laboratory-fixed angular momentum operators on the rigid rotor functions can be calculated (by ladder operators) as

$$\begin{aligned} \hat{J}_X |JKM\rangle &= \frac{1}{2} \sqrt{J(J+1) - M(M+1)} |JKM+1\rangle \\ &\quad + \frac{1}{2} \sqrt{J(J+1) - M(M-1)} |JKM-1\rangle \end{aligned} \quad (\text{S21})$$

$$\begin{aligned} \hat{J}_Y |JKM\rangle &= -\frac{i}{2} \sqrt{J(J+1) - M(M+1)} |JKM+1\rangle \\ &\quad + \frac{i}{2} \sqrt{J(J+1) - M(M-1)} |JKM-1\rangle \end{aligned} \quad (\text{S22})$$

$$\hat{J}_Z |JKM\rangle = M |JKM\rangle. \quad (\text{S23})$$

S3. FURTHER COMPUTATIONAL DETAILS AND CONVERGENCE TESTS

Throughout the computations the proton mass was $m_p = 1.007\,276\,466\,578\,9\text{ u}$, and the proton g factor was $g_p = 5.585\,694\,689\,3$ [45].

Table S1. Rotational energies up to $J = 3$ corresponding to the vibrational ground state computed with GENIUSH using the $r_{12}, r_{13}, \theta_{213}$ valence coordinates and the GLH3P PES [37]. For the r_{12} and r_{13} stretching degrees of freedom, we used PO-DVR constructed over a Laguerre DVR based on the $L_n^{(\alpha=2)}$ associated Laguerre polynomials, and 61 grid points scaled to the $[0.3, 6.5]$ bohr interval. For the $\cos \theta_{213}$ angle, we used Jacobi DVR based on the $J_n^{(\alpha=0.05, \beta=0.05)}$ Jacobi polynomials and 91 DVR points. This (61,61,91) grid was sufficient to converge the energies to 10^{-6} cm^{-1} (with the present PES). The MARVEL compilation of experimental data and the conventional (J, m) labelling of the rovibrational states are also reproduced from Ref. [40].

J	m	Γ	$\tilde{\nu}$ [cm^{-1}]	
			This work	MARVEL [40]
1	1	E''	64.128293876	64.121000
1	0	A'_2	86.966144514	86.960000
2	2	E'	169.308639849	169.294000
2	1	E''	237.368760616	237.357000
3	3	A'_2	315.364469199	315.354081
3	2	E'	428.041883665	428.019000
3	1	E''	494.792192357	494.773333
3	0	A'_2	516.907378512	516.878695

Table S2. Basis set dependence of the magnetic properties at the CCSD level: \mathcal{G} (dimensionless), isotropic \mathcal{M} in kHz, and isotropic σ in ppm (10^{-6}). $r_{12} = r_{13} = 1.65$ bohr and $\theta_{213} = 60^\circ$. The molecule is placed in the yz plane with the z axis parallel to the bisector of the $\text{H}_2\text{-H}_1\text{-H}_3$ angle.

	\mathcal{G}_{xx}	$\mathcal{G}_{yy/zz}$	\mathcal{M}	σ
cc-pVDZ	0.9791	0.9328	73.06	20.59
cc-pVTZ	0.9761	0.9249	70.79	20.55
aug-cc-pVTZ	0.9764	0.9265	70.76	20.55
cc-pVQZ	0.9764	0.9247	70.42	20.51

Table S3. Summary of the prefactors appearing in our computer implementation of Eqs. (5) and (6) with the coupling tensors taken as printed by CFOUR (or DALTON), the magnetic induction in Gauss (0.1 mT), and computing the rovibrational-hyperfine-magnetic energies in cm^{-1} .

	coefficients to cm^{-1}
Spin-rotation coupling matrix [kHz]	$-3.335\ 640\ 951\ 982 \cdot 10^{-8}$
Direct spin-spin coupling [bohr^{-3}]	$-2.703\ 907\ 337\ 273 \cdot 10^{-5}$
Indirect spin-spin coupling [Hz]	$3.335\ 640\ 951\ 981 \cdot 10^{-11}$
Rotation-magnetic coupling [dimensionless]	$-2.542\ 623\ 411\ 647 \cdot 10^{-8}$
Direct spin-magnetic coupling [dimensionless]	$1.420\ 231\ 808\ 733 \cdot 10^{-7}$
Spin-magnetic coupling [dimensionless]	$-1.420\ 231\ 808\ 733 \cdot 10^{-7}$

Table S4. Character table and irrep labels of the S_3 permutational group. The labelling follows that of $D_{3h}(\text{M})$ [61], but since space inversion is not considered, we dropped the ' and ' superscripts from the $D_{3h}(\text{M})$ irrep labels.

	Classes: E $\{P_{123}, P_{132}\}$ $\{P_{12}, P_{13}, P_{23}\}$		
A_1	1	1	1
A_2	1	1	-1
E	2	-1	0

We used the following spin-1/2 angular momentum operators,

$$\hat{I}_X = \frac{1}{2} \begin{pmatrix} 0 & 1 \\ 1 & 0 \end{pmatrix} \quad \hat{I}_Y = \frac{1}{2} \begin{pmatrix} 0 & i \\ -i & 0 \end{pmatrix} \quad \hat{I}_Z = \frac{1}{2} \begin{pmatrix} -1 & 0 \\ 0 & 1 \end{pmatrix}. \quad (\text{S24})$$

S4. A SIMPLE ANALYTIC REPRESENTATION OF THE ELECTRIC DIPOLE POLARIZABILITY MATRIX

The following functional form was used to fit the electric dipole polarizability computed with electronic structure theory and rotated to the bisector embedding used in the rovibrational part. The α_{ij} ($i, j = x, y, z$) matrix is symmetric, and $\alpha_{xy} = \alpha_{xz} = 0$ in our bisector embedding. The following functions were used for α_{xx} , α_{yy}

and α_{zz} , ($i = x, y, z$)

$$\begin{aligned} & \alpha_{ii}(r_{12}, r_{13}, \theta_{213}) \\ &= \sum_{n_{r_{12}}=0}^{14} \sum_{n_{r_{13}}=0}^{14} \sum_{n_{\theta_{213}}=0}^{17} H_{n_{r_{12}}, n_{r_{13}}, n_{\theta_{213}}}^{(ii)} (r_{12} - 2.5)^{n_{r_{12}}} (r_{13} - 2.5)^{n_{r_{13}}} (\theta_{213} - 60)^{n_{\theta_{213}}} , \end{aligned} \quad (\text{S25})$$

and for the non-zero off-diagonal element,

$$\begin{aligned} & \alpha_{yz}(r_{12}, r_{13}, \theta_{213}) \\ &= \sum_{n_{r_{12}}=0}^{14} \sum_{n_{r_{13}} \neq n_{r_{12}}=0}^{14} \sum_{n_{\theta_{213}}=0}^{17} H_{n_{r_{12}}, n_{r_{13}}, n_{\theta_{213}}}^{(yz)} (r_{12} - 2.5)^{n_{r_{12}}} (r_{13} - 2.5)^{n_{r_{13}}} (\theta_{213} - 60)^{n_{\theta_{213}}} . \end{aligned} \quad (\text{S26})$$

S5. PAULI-ALLOWED STATES: CALCULATION OF THE EFFECT OF THE P_{23} PERMUTATION OPERATOR

In this work, we used PO-DVR for r_{12} and r_{13} in the (ro)vibrational computations, and we need to carry out the symmetry analysis over the quadrature grid. The proton-spin-rovibrational wave functions (under the effect of an external magnetic field) transform according to the irreps of the S_3 permutation group. Only the states of A_2 symmetry fulfil the Pauli principle, *i.e.*, anti-symmetry upon the exchange of any pairs of protons. A_2 is a one-dimensional irrep, and therefore, all the rovibrational-spin wave functions allowed by the Pauli principle are singly degenerate (though accidental degeneracies may occur). So, we first identify the singly degenerate rovibrational-hyperfine-Zeeman states, and then, check whether they change sign upon the action of one (any) of the particle exchange operations. In the present coordinate and grid representation, the effect of the P_{23} permutation can be calculated, which is outlined in the following paragraphs.

The rovibrational-spin wave functions are expanded as the linear combination of the product of functions,

$$\Phi_{J, n_J, \tilde{K}, \tau}(r_{12}, r_{13}, \cos \theta_{213}) |J, \tilde{K}, \tau, M\rangle_{\Omega} |I_i\rangle . \quad (\text{S27})$$

The effect of P_{23} can be straightforwardly calculated if all factors are eigenfunctions

of P_{23} . In the case of the one-dimensional irreps, the effect of P_{23} is

$$P_{23}\Phi_{J,n_J,\tilde{K},\tau}(r_{12}, r_{13}, \cos \theta_{213}) = \pm \Phi_{J,n_J,\tilde{K},\tau}(r_{12}, r_{13}, \cos \theta_{213}) \quad (\text{S28})$$

$$P_{23}|J, \tilde{K}, \tau, M\rangle = \pm |J, \tilde{K}, \tau, M\rangle \quad (\text{S29})$$

$$P_{23}|I_i\rangle = \pm |I_i\rangle, \quad (\text{S30})$$

where we used the linear combination of the eight spin functions that are eigenfunctions of P_{23} ,

$$\begin{aligned} |I_1\rangle &= |\alpha, \alpha, \alpha\rangle \\ |I_2\rangle &= \frac{1}{\sqrt{2}}(|\alpha, \alpha, \beta\rangle + |\alpha, \beta, \alpha\rangle) \\ |I_3\rangle &= \frac{1}{\sqrt{2}}(|\alpha, \alpha, \beta\rangle - |\alpha, \beta, \alpha\rangle) \\ |I_4\rangle &= |\alpha, \beta, \beta\rangle \\ |I_5\rangle &= |\beta, \alpha, \alpha\rangle \\ |I_6\rangle &= \frac{1}{\sqrt{2}}(|\beta, \alpha, \beta\rangle + |\beta, \beta, \alpha\rangle) \\ |I_7\rangle &= \frac{1}{\sqrt{2}}(|\beta, \alpha, \beta\rangle - |\beta, \beta, \alpha\rangle) \\ |I_8\rangle &= |\beta, \beta, \beta\rangle. \end{aligned} \quad (\text{S31})$$

Regarding degenerate pairs (labelled with a and b) of rovibrational states, the $(\tilde{K}\tau)$ vibrational blocks, $\Phi_{J,n_{J,a},\tilde{K},\tau}(r_{12}, r_{13}, \cos \theta_{213})$ and $\Phi_{J,n_{J,b},\tilde{K},\tau}(r_{12}, r_{13}, \cos \theta_{213})$ are not necessarily symmetric or antisymmetric to P_{23} . But since the states are degenerate, we are free to choose any linear combination of them. So we choose the linear combination for which the matrix representation of P_{23} is diagonal,

$$|J, n_{J,1}, M\rangle = \cos \phi |J, n_{J,a}, M\rangle + \sin \phi |J, n_{J,b}, M\rangle \quad (\text{S32})$$

and

$$|J, n_{J,2}, M\rangle = -\sin \phi |J, n_{J,a}, M\rangle + \cos \phi |J, n_{J,b}, M\rangle \quad (\text{S33})$$

with

$$\begin{aligned} P_{23}|J, n_{J,1}, M\rangle &= |J, n_{J,1}, M\rangle \\ P_{23}|J, n_{J,2}, M\rangle &= -|J, n_{J,2}, M\rangle . \end{aligned} \tag{S34}$$

Regarding the rotational basis functions, the effect of P_{23} on the bisector embedding (Fig. 1) used in this work is the change of γ to $\gamma + \pi$, which translates to

$$P_{23}|J, K, M\rangle_{\Omega} = (-1)^K |J, K, M\rangle_{\Omega} \tag{S35}$$

and

$$P_{23}|J, \tilde{K}, \tau, M\rangle_{\Omega} = (-1)^{\tilde{K}} |J, \tilde{K}, \tau, M\rangle_{\Omega} . \tag{S36}$$

With these considerations, the effect of P_{23} can be determined for each factor in the basis set expansion, Eq. (S27), and the states can be assigned to A_1 or A_2 symmetry without ambiguity. The only ambiguity remains with the identification of the singly degenerate proton-spin-rovibrational states (in an external magnetic field), since accidental degeneracies may occur. In future work, we will implement the full S_3 projector, which will provide a fully automated and robust selection of the Pauli allowed subspace, by using the Pekeris coordinates [62, 63] or transformation to FBR (of another DVR computation).